Novel Red-Emitting Phosphor $Ca_9Y(PO_4)_7:Ce^{3+},Mn^{2+}$ with Energy Transfer for Fluorescent Lamp Application

Chien-Hao Huang, Te-Wen Kuo, and Teng-Ming Chen*

Phosphors Research Laboratory and Department of Applied Chemistry, National Chiao Tung University, Hsinchu 30010, Taiwan

ABSTRACT A series of new luminescent emission-tunable phosphors $Ca_9Y(PO_4)_7:zCe^{3+},xMn^{2+}$ have been synthesized by a high-temperature solid-state reaction. We report a broad deep red-emitting composition-optimized phosphor $(Ca_{0.9})_9Y_{0.85}(PO_4)_7$: $0.15Ce^{3+},0.1Mn^{2+}$, which has been found to be feasible for the application in fluorescent lamps. The Commission Internationale de l'Eclairage (CIE) chromaticity coordinates measured for the phosphor were (0.68, 0.29), and those for fluorescent lamps with and without a 600 nm filter were found to be (0.67, 0.29) and (0.54, 0.32), respectively. The $Ca_9Y(PO_4)_7:Ce^{3+},Mn^{2+}$ phosphor showed two emission bands under 254 nm excitation: the one observed at 366 nm was attributed to Ce^{3+} ion emission, and the other found at 650 nm was assigned to the emission from Mn^{2+} ions. We have shown that the mechanism of energy transfer from Ce^{3+} to Mn^{2+} was of the resonance type and it occurred via an electric dipole-quadrupole interaction. Furthermore, we have calculated the critical distance for $Ce^{3+} \rightarrow Mn^{2+}$ energy transfer to be 13.45 Å by concentration quenching methods.

KEYWORDS: $Ca_9Y(PO_4)_7:Ce^{3+},Mn^{2+}$ • photoluminescence • energy transfer • fluorescent lamps

INTRODCUCTION

Most applications that employ red oxide phosphors suffer from problems such as low color purity. For example, a plasma display panel (PDP) can not generate a purely deep red color because the CIE chromaticity y-coordinate value of red-emitting borate phosphors, known as the most widely used for PDPs, is deviated from the standard value (0.67) specified by the National Television Standard Committee (NTSC). At best, the value is around 0.65. A similar problem is now being addressed in the case of fluorescent lamps (FLs) and light-emitting diode (LED) lamps that have been developed for application in back light units (BLUs) in liquid-crystal displays (LCDs). In this regard, a deep red phosphor based on a Ce^{3+}- and Mn^{2+}-codoped $Ca_9Y(PO_4)_7$ system has been examined in the present investigation. The phosphor will be highly beneficial for improving color purity when used as an emitted material in FLs.

The energy transfer from sensitizer to activator by rare earth ions has been an important research field. Mn^{2+}-doped luminescent materials have been known to show broadband emissions from 500 to 700 nm depending on the crystal field of the host materials (1−3). Although these luminescent materials could be good candidates for red phosphors, their disadvantage is that the d−d absorption transition of Mn^{2+} ions is strongly parity forbidden, and therefore, the ions are difficult to pump. As a promising sensitizer for Mn^{2+} ions, Ce^{3+} has been widely used in many Mn^{2+}-doped hosts such as $MgSiN_2$ (4), $BaAl_2O_4$ (5), $CaSiO_3$ (6), Zn_2SiO_4 (7), $Zn(PO_3)_2$ (8), and $Ba_2Ca(BO_3)_2$ (9) to improve the emission intensity of Mn^{2+}. Ye et al. and Kim et al. have observed effective energy transfer from Eu^{2+} to Mn^{2+} in $BaMg_2Si_2O_7$ (10) and $Ba_3MgSi_2O_8$ (11) where Mn^{2+} shows red emission. To the best of our knowledge, the luminescence properties of $Ca_9Y(PO_4)_7:Ce^{3+},Mn^{2+}$ have not been reported in the literature. In this study, we report an unprecedented emission-tunable deep red-emitting phosphor, $Ca_9Y(PO_4)_7:Ce^{3+},Mn^{2+}$. We have systematically investigated the energy transfer mechanism between Ce^{3+} and Mn^{2+} in this phosphor by calculating the exact value of the critical energy transfer distance (R_c) between the Ce^{3+} and Mn^{2+} ions.

$Ca_9Y(PO_4)_7$, which is isostructural to β-$Ca_9In(PO_4)_7$, crystallizes in a rhombohedral unit cell with the space group $R3c$ (No. 161) (12) and unit-cell dimensions of $a = 10.4442$ Å, $c = 37.324$ Å, $V = 3525.89$ Å^3, and $Z = 6$. All three crystallographically independent Ca^{2+} ions of $Ca_9Y(PO_4)_7$ have different coordination environments: the one for Ca(1) is nine-coordinated, and those for Ca(2) and Ca(3) are both eight-coordinated. The crystal lattice has two more crystallographically independent cation sites (Y^{3+} and P^{5+}): the one for Y^{3+} is six-coordinated and three for P^{5+} are four-coordinated. The ionic radii for six-coordinated Y^{3+} and eight-coordinated Ca^{2+} are 0.9 and 1 Å, respectively; the ionic radii for six-coordinated Ce^{3+} and eight-coordinated Mn^{2+} are 1.01 and 0.96 Å, respectively. Therefore, on the basis of the effective ionic radii of cations with different coordination numbers (13), we have predicted that Ce^{3+} would occupy the Y^{3+} lattice sites and, as revealed by the emission decay lifetime data, Mn^{2+} would randomly occupy the three different Ca^{2+} lattice sites in the host structure.

* Corresponding author. E-mail: tmchen@mail.nctu.edu.tw. Tel: +886-35731695.

Received for review January 16, 2010 and accepted April 6, 2010

DOI: 10.1021/am100043q

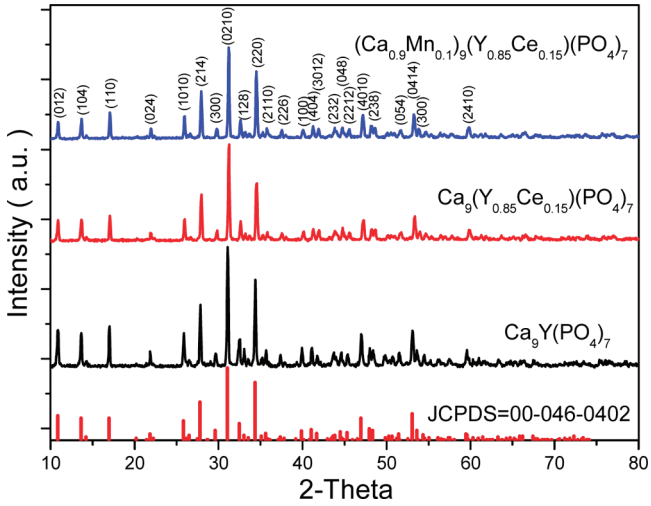

FIGURE 1. Powder XRD patterns of CYP (JCPDS 00-046-0402), CYP, CYP:Ce^{3+} and CYP:Ce^{3+},Mn^{2+}.

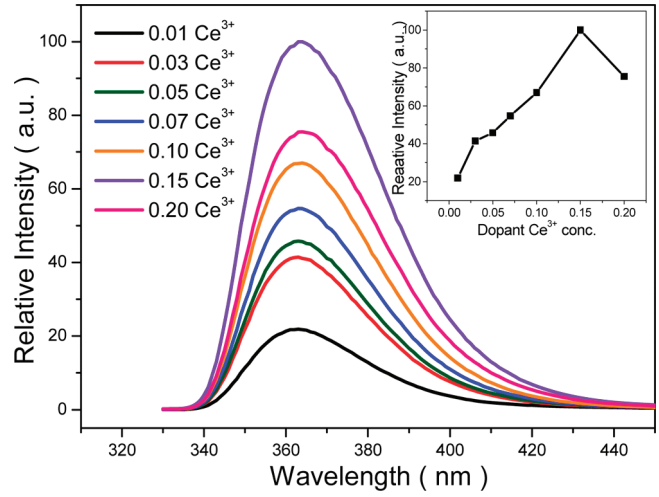

FIGURE 2. Concentration dependence of relative PL intensity of CYP:zCe^{3+} (z = 0.01−0.2) under 254 nm excitation.

EXPERIMENTAL SECTION

Two series of phosphors with compositions of $Ca_9Y(PO_4)_7$:zCe^{3+} (CYP:zCe^{3+}) and $Ca_9Y(PO_4)_7$:zCe^{3+},xMn^{2+} (CYP:zCe^{3+},xMn^{2+}) with high purity were prepared by heating a mixture of stoichiometric raw materials of $CaCO_3$, Y_2O_3, $(NH_4)_2HPO_4$, CeO_2, and MnO (all in purity >99.9%) at 1200 °C for 8 h. The obtained samples were then reduced at 1000°C for 8 h under a 15% H_2/85% N_2 atmosphere. The phase purity and crystal structure of the powder were examined by powder X-ray diffraction (XRD) profiles, which were measured with a Bruker AXS D8 advanced automatic diffractometer with Cu Kα radiation operated at 40 kV and 40 mA. The photoluminescence (PL) and PL excitation (PLE) spectra for CYP:Ce^{3+},Mn^{2+} phosphors were obtained with a Spex Fluorolog-3 spectrofluorometer (Instruments S.A., NJ) equipped with a 450-W Xe light source and double excitation monochromators.

Time-resolved measurements were performed with a tunable nanosecond optical-parametric-oscillator/Q-switch-pumped YAG:Nd^{3+} laser system (NT341/1/UV, Ekspla). Emission transients were collected with a nanochromater (SpectraPro-300i, ARC), detected with photomultiplier tube (R928HA, Hamamatsu), connected to a digital oscilloscope (LT372, LeCrop) and transferred to a computer for kinetics analysis. The Commission International de l'Eclairage (CIE) chromaticity coordinates for all samples were measured by a Laiko DT-101 color analyzer equipped with a CCD detector (Laiko Co., Tokyo, Japan).

RESULTS AND DISCUSSION

The XRD patterns of CYP, CYP:Ce^{3+}, and CYP:Ce^{3+},Mn^{2+} are shown in Figure 1. They were found to be consistent with that reported in JCPDS file no. 00-046-0402 (14). The XRD analysis was performed to determine the chemical purity and phase homogeneity of the CYP:Ce^{3+},Mn^{2+} phosphor. The lattice parameters of CYP, CYP:0.15Ce^{3+}, and CYP:0.15Ce^{3+},0.1Mn^{2+} phases were calculated based on the experimental XRD profiles with cell refinement software. The lattice parameters of CYP powder were found to be $a = b = 10.425(8)$ Å, $c = 37.3042(10)$ Å, $V = 3510.8$ Å^3. As Y^{3+} was substituted by a larger Ce^{3+} ion in CYP host, the lattice parameters of CYP:0.15Ce^{3+} became $a = b = 10.453(2)$ Å, $c = 37.4213(5)$ Å, V = 3541.1 Å^3. Furthermore, as Ca^{2+} was substituted by a small Mn^{2+} ion in CYP:0.15Ce^{3+} host, the lattice parameters of CYP:0.15Ce^{3+},0.1Mn^{2+} were found to shrink to $a = b = 10.401$ (3) Å, $c = 37.2026(5)$ Å, $V = 3485.7$ Å^3. These results indicated that Ce^{3+} and Mn^{2+} ions were undoubtedly doped into and entered the CYP crystal lattice.

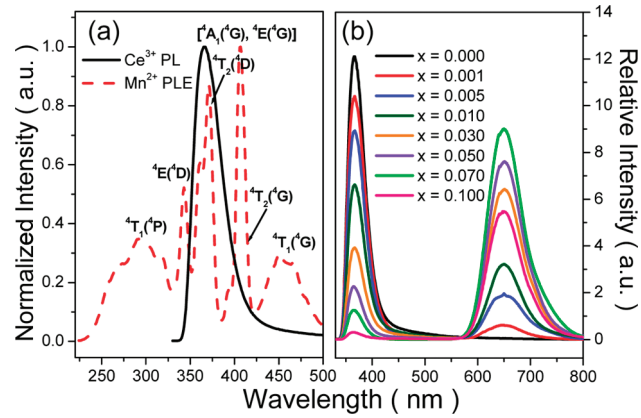

FIGURE 3. (a) Spectral overlap between PL spectrum of CYP:Ce^{3+} (solid line) and PLE spectrum of CYP:Mn^{2+} (dashed line). (b) PL spectra of CYP:0.15Ce^{3+},xMn^{2+} phosphors excited at 254 nm.

The concentration dependence of relative PL intensity of CYP:zCe^{3+} (z = 0.01−0.2) under 254 nm excitation was demonstrated in Figure 2. The PL spectra exhibited a broad band UV emission centered at 366 nm, which was imputed to the $5d^1 \rightarrow 4f^1$ of the Ce^{3+} ion. The optimal Ce^{3+} dopant content was found to be 0.15 mol per formula unit and the PL intensity was observed to increase with increasing z when $z < 0.15$. For samples with Ce^{3+} dopant content higher than 0.15, concentration quenching was observed and the PL intensity was found to decrease with increasing Ce^{3+} dopant content.

Figure 3a shows the spectral overlap between the PL spectrum of Ce^{3+} (solid line) and the PLE spectrum of Mn^{2+} (dashed line). The PL spectrum showed an intense broadband emission centered at 366 nm, which was assigned to the $5d^1 \rightarrow 4f^1$ transition of CYP:Ce^{3+}. The PLE spectrum of CYP:Mn^{2+} showed several bands centered at 291, 343, 372, 407, 418, and 450 nm, corresponding to the transitions from the $^6A_1$ (^6S) level to the $^4T_1$ (^4P), ^4E (^4D), $^4T_2$ (^4D), [$^4A_1$ (^4G), ^4E (^4G)], $^4T_2$ (^4G), and $^4T_1$ (^4G) levels, respectively (15, 16). This result can be a good indicator of the energy transfer from

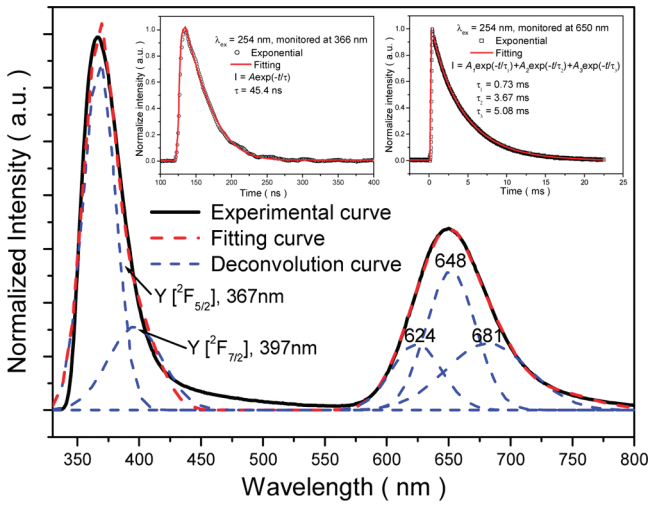

FIGURE 4. Experimental spectrum (solid line), fitted curve (red dashed line), and deconvoluted Gaussian components (blue dashed lines) of CYP:0.15Ce^{3+}, 0.01Mn^{2+}.

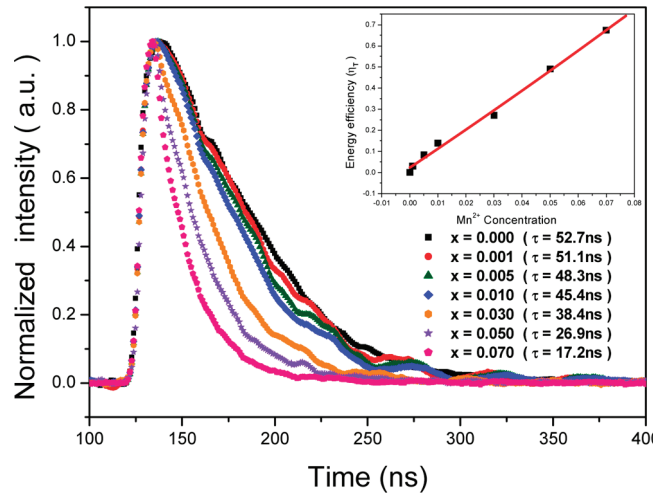

FIGURE 5. Decay curves of Ce^{3+} emission in CYP:0.15Ce^{3+},xMn^{2+} excited at 254 nm and monitored at 366 nm. The inset shows the energy transfer efficiency under 254 nm excitation.

Ce^{3+} to Mn^{2+} in CYP:0.15Ce^{3+},xMn^{2+}. Figure 3b shows PL spectra of CYP:0.15Ce^{3+},xMn^{2+} excited at 254 nm. The intensity of Ce^{3+} emission at 366 nm decreased with an increasing doped Mn^{2+} concentration. In contrast, the PL intensity of Mn^{2+} emission increased at 650 nm when the Mn^{2+} concentration quenching was above 0.07 mol. The observed variations in the emission intensities of Ce^{3+} and Mn^{2+} in CYP:0.15Ce^{3+},xMn^{2+} (x = 0.001−0.1) strongly indicate the continuous energy transfer from Ce^{3+} to Mn^{2+}.

As shown in Figure 4, under 254 nm excitation, the emission spectrum of CYP:0.15Ce^{3+},0.01Mn^{2+} shows three broad emission bands. The band centered at 366 nm was assigned to the 5d^1 → 4f^1 transition of Ce^{3+}, and a band centered at 650 was attributed to the 3d → 3d transitions of Mn^{2+}. The asymmetric UV emission band was attributed to the spin-orbit coupling of the 4f^1 ground state of Ce^{3+}, which split into two levels (^{2}F$_{5/2}$ and ^{2}F$_{7/2}$) (17), and the occupation of Ce^{3+} in an independent Y^{3+} site. By Gaussian deconvolution (18, 19), this emission spectrum can be decomposed into two Gaussian profiles with peaks centered at 367 and 397 nm (Figure 4, red dashed lines), respectively, that can be attributed to transitions from the lowest 5d level to the ^{2}F$_{5/2}$ and ^{2}F$_{7/2}$ levels for Ce^{3+}, respectively. The energy difference between spin-orbit splitting of the 4f ground state in CYP:0.15Ce^{3+} was about 2059 cm^{-1}, which was in good agreement with the theoretical value of 2000 cm^{-1} (20). In addition, the symmetric red emission band originating from the occupation of three different Ca^{2+} sites by Mn^{2+} was deconvoluted into three peaks centered at 624, 648, and 681 nm, respectively (Figure 4, blue dashed lines). The inset shows the decay lifetime of CYP:0.15Ce^{3+},0.01Mn^{2+} phosphor excited at 254 nm, monitored at 366 nm and 650 nm, respectively. The results revealed that Ce^{3+} only occupied the Y^{3+} site and did not occupy the Ca^{2+} site since it was best fitted with only one decay constant τ_1= 45.4 ns. When the Mn^{2+} emission at 650 nm was monitored, we have obtained three decay constants τ_1= 0.73 ms, τ_2= 3.67 ms, and τ_3= 5.08 ms, which are attributed to the Mn^{2+} substitution for three different Ca^{2+} sites, respectively. These results further support the validity of spectral deconvolution and similar methods have been used and reported by Shon et al. (21), Tang et al. (22), Zhang et al. (23), and Ding et al. (24).

Furthermore, the decay curves of CYP:0.15Ce^{3+},xMn^{2+} phosphors excited at 254 nm and monitored at 366 nm are shown in Figure 5. The decay curves were well fitted by a single exponential equation (25)

$$I = A_1\exp(-t/\tau_1) \quad (1)$$

where I is the luminescence intensity monitored at 366 nm, A_1 is constant, t is the time, and τ_1 is the decay constant for the exponential component. As shown in Figure 5, by curve fitting using the above equation, the decay constant τ_1 for Ce^{3+} emission reduced monotonically from 52.7 to 17.2 ns as x increased from 0 to 0.07. The energy transfer efficiency (η_T) from a sensitizer to an activator can be calculated by using the following formula suggested by Paulose et al. (26) and Tang and Shi (27).

$$\eta_T = 1 - \frac{\tau_S}{\tau_{S0}} \cong 1 - \frac{I_S}{I_{S0}} \quad (2)$$

where τ_{S0} and τ_S are the decay lifetimes of the sensitizer (Ce^{3+}) in the absence and presence of the activator (Mn^{2+}), respectively. I_{S0} and I_S are the luminescence intensities of the sensitizer Ce^{3+} in the absence and presence of the activator Mn^{2+}, respectively. η_T, the energy transfer efficiency from Ce^{3+} to Mn^{2+} in CYP:0.15Ce^{3+},xMn^{2+}, calculated as a function of x, is shown in the inset of Figure 5. η_T was found to increase with an increasing Mn^{2+} dopant content.

On the bais of the Dexter's energy transfer formula of multipolar interaction and Reisfeld's approximation, the following relation can be obtained (28, 29)

$$\frac{\eta_{S0}}{\eta_S} \propto C^{\alpha/3} \text{and} \frac{I_{S0}}{I_S} \propto C^{\alpha/3} \quad (3)$$

where η_{S0} and η_S are the luminescence quantum efficiencies of Ce^{3+} in the absence and presence of Mn^{2+}, respectively; the value of η_{S0}/η_S can be approximately estimated from the luminescence intensity ratio (I_{S0}/I_S); C is the concentration of Mn^{2+}; and $\alpha = 6$, 8, and 10 for dipole−dipole, dipole−quadrupole, and quadrupole−quadrupole interactions, respectively. Equations 2 and 3 can thus be represented by the follow equation

$$\frac{\tau_{S0}}{\tau_S} \propto C^{\alpha/3} \quad (4)$$

Plots of τ_{S0}/τ_S and $C^{\alpha/3}$ based on above equation are also shown in Figures 6a−c. Linear behavior was observed only when $\alpha = 8$, implying that energy transfer from Ce^{3+} to Mn^{2+} occurred via the dipole-quadrupole mechanism. The critical distance R_c for the energy transfer from Ce^{3+} to Mn^{2+} was calculated using the concentration quenching method.

The critical distance R_{Ce-Mn} between Ce^{3+} and Mn^{2+} can be estimated using the relation given by Blasse (25)

$$R_{Ce-Mn} = 2\left[\frac{3V}{4\pi x_c N}\right]^{1/3} \quad (5)$$

where x_c is the critical concentration, N is the number of Z ions in the unit cell, and V is the volume of the unit cell. For the $Ca_9Y(PO_4)_7$ crystal, the analytical and experimental values were $N = 6$ and $V = 3525.89$ Å^3. Thus, the R_{Ce-Mn} of CYP:0.15Ce^{3+},$x$$Mn^{2+}$ was determined to be 19.18, 17.92, 16.72, 13.87, 12.32, 11.29, and 10.22 Å for $x = 0.001$, 0.005. 0.01, 0.03, 0.05, 0.07, and 0.1, respectively. The critical concentration at which the luminescence intensity of Ce^{3+} was half of that in samples without Mn^{2+} was 0.461. Therefore, the critical distance (R_c) of energy transfer was calculated to be 13.45 Å. We also observed that radiative emission from Ce^{3+} prevailed when $R_{Ce-Mn} > R_c$, whereas energy transfer from Ce^{3+} to Mn^{2+} dominated when $R_{Ce-Mn} < R_c$ (3).

The CIE chromaticity diagram for CYP:0.15Ce^{3+},$x$$Mn^{2+}$ phosphors was measured at different x values, as shown in Figure 7. The CIE coordinates varied systematically between (0.15, 0.11), (0.24, 0.14), (0.28, 0.16), (0.35, 0.19), (0.51, 0.24), (0.61, 0.27), (0.67, 0.29), and (0.68, 0.29) for $x = 0$, 0.001, 0.005. 0.01, 0.03, 0.05, 0.07, and 0.1, corresponding to hues ranging from UV to deep red. The inset shows a magnified view of the CIE chromaticity diagram of the CYP:0.15Ce^{3+},0.1Mn^{2+} deep red phosphor under 254 nm excitation. Shown in Figure 8 are the PL spectra and quantum efficiency of CYP:0.15Ce^{3+},0.1Mn^{2+} and commercial red phosphor 3.5MgO · 0.5MgF_2 · GeO_2:Mn^{4+} (Nichia NP320) under 254 nm excitation. The external quantum efficiency of CYP:0.15Ce^{3+},0.1Mn^{2+} and 3.5MgO · 0.5MgF_2 · GeO_2:

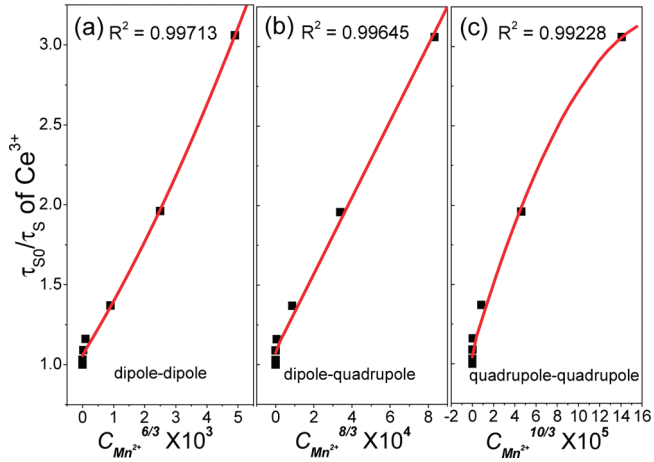

FIGURE 6. Dependence of τ_{S0}/τ_S of Ce^{3+} on (a) $C^{6/3}$, (b) $C^{8/3}$, and (c) $C^{10/3}$.

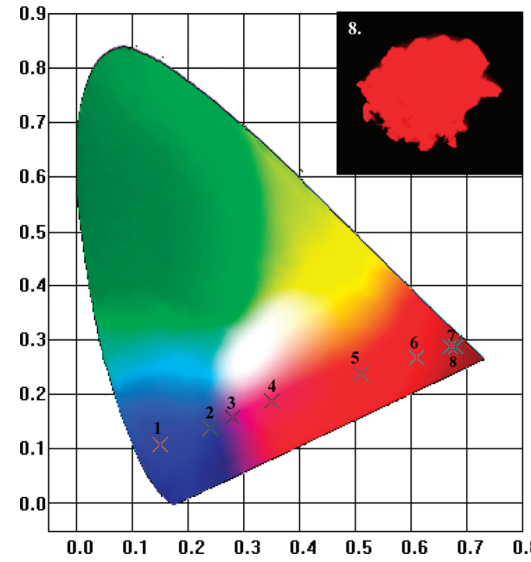

FIGURE 7. Evolution of CIE chromaticity coordinates for CYP: 0.15Ce^{3+},$x$$Mn^{2+}$ excited at 254 nm. The inset shows the appearance of the CYP:0.15Ce^{3+},0.1Mn^{2+} phosphor under 254 nm excitation.

Mn^{4+} phosphor were found to be 55.13 and 31.11%. Furthermore, the emission wavelength and CIE chromaticity coordinates for CYP:0.15Ce^{3+},0.1Mn^{2+} and 3.5MgO · 0.5MgF_2 · GeO_2:Mn^{4+} were observd to be 650 nm (0.68, 0.29) and 659 nm (0.71, 0.28), respectively.

We have tested a low-pressure mercury vapor fluorescent lamp (FL) derived from the CYP:0.15Ce^{3+}, 0.1Mn^{2+} phosphor. The FL consisted of a lamp envelope whose inner surface was coated with a layer of the luminescent phosphor for generating ultraviolet radiation and a pair of discharge electrodes arranged at the sealed ends of the lamp envelope. When a power of 8 W was applied to the cathodes for inducing discharge, thereby emitting ultraviolet light from mercury, the excited fluorescent layer efficiently emitted deep red light with a main peak wavelength at around 650 nm (Figure 9). The spectrum measured without any filter showed peaks centered at 405, 436, 546, and 578 nm for mercury (30). The CIE coordinates (x,y) for FLs with and without a 600 nm filter were determined to be (0.5417,

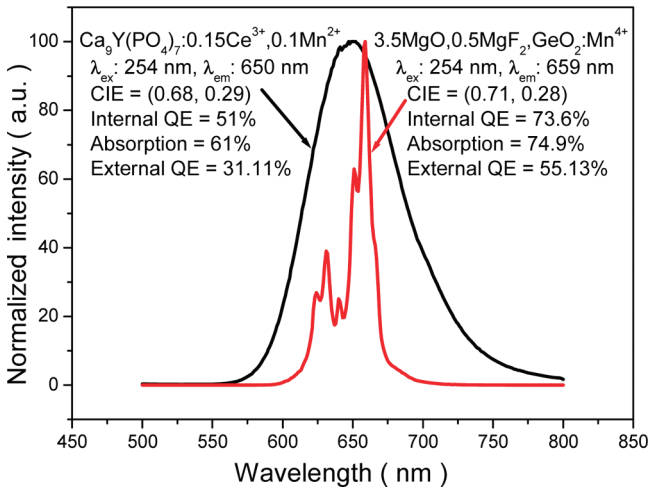

FIGURE 8. Comparison of PL spectrum and quantum efficiency of CYP:0.15Ce^{3+},0.1Mn^{2+} and commercial red phosphor 3.5MgO · 0.5MgF_2 · GeO_2:Mn^{4+} (Nichia NP320) under 254 nm excitation.

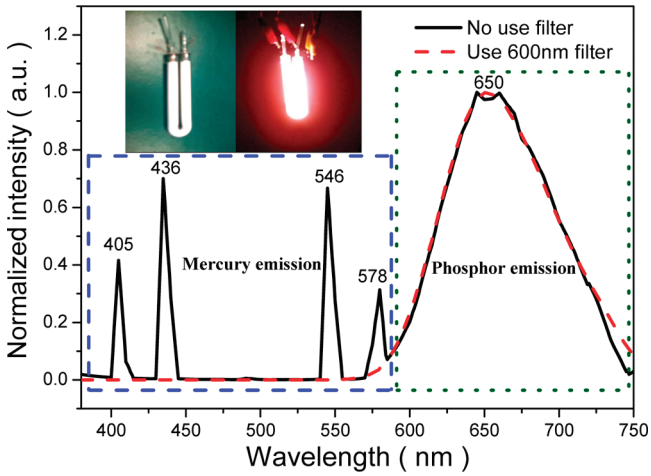

FIGURE 9. PL spectrum of FL fabricated using mercury vapor and CYP:0.15Ce^{3+},0.1Mn^{2+} phosphor in sealed glass tube. The inset shows the operation of FLs at an applied power of 8 W.

0.3164) and (0.6716, 0.2893), as compared to the NTSC red (0.67, 0.33), respectively.

CONCLUSIONS

In conclusion, a class of new luminescent material CYP: 0.15Ce^{3+},xMn^{2+} has been synthesized by a high-temperature solid-state reaction. We have prepared CYP: 0.15Ce^{3+},0.1Mn^{2+} phosphors and found them to be feasible for use in red fluorescent lamps. When a power of 8 Watt was applied to the cathodes for inducing discharge, thereby emitting ultraviolet light from mercury, the excited fluorescent layer efficiently emitted deep red light with a main peak wavelength at around 650 nm. The measured CIE chromaticity coordinates (*x*, *y*) for FLs with and without a 600-nm filter have been found to be (0.67, 0.29) and (0.54, 0.32), respectively. The $Ce^{3+} \rightarrow Mn^{2+}$ energy transfer was demonstrated to be attributable to an electric dipole−quadrupole interaction, and the critical distance of energy transfer from Ce^{3+} to Mn^{2+} has been calculated to be about 13.45 Å by concentration quenching methods.

Acknowledgment. This research was supported by National Science Council of Taiwan under Contract NSC98-2113-M-009-005-MY3 (T.-M.C. and C.-H.H.).

REFERENCES AND NOTES

(1) Chang, C. K.; Chen, T. M. *Appl. Phys. Lett.* **2007**, *90*, 161901.
(2) Yang, W. J.; Chen, T. M. *Appl. Phys. Lett.* **2006**, *88*, 101903.
(3) Yang, W. J.; Luo, L.; Chen, T. M.; Wang, N. S. *Chem. Mater.* **2005**, *17*, 3883.
(4) Kulshreshtha, C.; Kwak, J. H.; Park, Y. J.; Sohn, K. S. *Opt. Lett.* **2009**, *34*, 794.
(5) Suriyamurthy, N.; Panigrahi, B. S. *J. Lumin.* **2007**, *127*, 483.
(6) Zhang, X.; Liu, X. *Chin. J. Lumin.* **1992**, *13*, 1.
(7) Wang, L.; Liu, X.; Hou, Z.; Li, C.; Yang, P.; Cheng, Z.; Lian, H.; Lin, J. *J. Phys. Chem.* **2008**, *112*, 18882.
(8) Caldiño, U.; Hernández-Pozos, J. L.; Flores, C.; Speghini, A.; Bettinelli, M. *J. Phys.: Condens. Matter* **2005**, *17*, 7297.
(9) Guo, C.; Luan, L.; Xu, Y.; Gao, F.; Liang, L. *J. Electrochem. Soc.* **2008**, *155*, J310.
(10) Ye, S.; Zhang, J.; Zhang, X.; Lu, S.; Ren, X.; Wang, X. *J. Appl. Phys.* **2007**, *101*, 033513.
(11) Kim, J. S.; Lim, K. T.; Jeong, Y. S.; Jeon, P. E.; Choi, J. C.; Park, H. L. *Solid State Commun.* **2005**, *135*, 21.
(12) Morozov, V. A.; Belik, A. A.; Stefanovich, S. Yu.; Grebenev, V. V.; Lebedev, O. I.; Tendeloo, G. V.; Lazoryak, B. I. *J. Solid State Chem.* **2002**, *165*, 278.
(13) Shannon, R. D. *Acta Crystallogr., Sect. A* **1976**, *32*, 751.
(14) *JCPDS file no. 00-046-0402*; International Centre for Diffraction Data: Newtown Square, PA.
(15) Huang, C. H.; Chen, T. M.; Liu, W. R.; Chiu, Y. C.; Yeh, Y. T.; Jang, S. M. *Appl. Mater. Interface* **2010**, *2*, 259.
(16) Huang, C. H.; Chen, T. M. *Opt. Express* **2010**, *18*, 5089.
(17) Wang, Z. L.; Quan, Z. W.; Jia, P. Y.; Lin, C. K.; Luo, Y.; Chen, Y.; Fang, J.; Zhou, W.; O'Connor, C. J.; Lin, J. *Chem. Mater.* **2006**, *18*, 2030.
(18) Liu, W. R.; Chiu, Y. C.; Yeh, Y. T.; Jang, S. M.; Chen, T. M. *J. Electrochem. Soc.* **2009**, *156*, J165.
(19) Wu, Z.; Gong, M.; Shi, J.; Wang, G.; Su, Q. *Chem. Lett.* **2007**, *36*, 410.
(20) Yu, M.; Lin, J.; Fu, J.; Zhang, H. J.; Han, Y. C. *J. Mater. Chem.* **2003**, *13*, 1413.
(21) Shon, K. S.; Cho, S. H.; Park, S. S.; Shin, N. *Appl. Phys. Lett.* **2006**, *89*, 051106.
(22) Tang, Y. S.; Hu, S. F.; Ke, W. C.; Lin, C. C.; Bagkar, N. C.; Liu, R. S. *Appl. Phys. Lett.* **2008**, *93*, 131114.
(23) Zhang, X.; Chen, H.; Ding, W.; Wu, H.; Kim, J. *J. Am. Ceram. Soc.* **2009**, *92*, 429.
(24) Ding, W.; Wang, J.; Liu, Z.; Zhang, M.; Su, Q.; Tang, J. *J. Electrochem. Soc.* **2008**, *155*, J122.
(25) Pang, R.; Li, C.; Shi, L.; Su, Q. *J. Phys. Chem. Solids* **2009**, *70*, 303.
(26) Paulose, P. I.; Jose, G.; Thomas, V.; Unnikrishnan, N. V.; Warrier, M. K. R. *J. Phys. Chem. Solids* **2003**, *64*, 841.
(27) Tan, Y.; Shi, C. *J. Phys. Chem. Solids* **1999**, *60*, 1805.
(28) Dexter, D. L. *J. Chem. Phys.* **1953**, *21*, 836.
(29) Blasse, G. *Philips. Res. Rep.* **1969**, *24*, 131.
(30) Sansonetti, C. J.; Salit, M. L.; Reader, J. *Appl. Opt.* **1996**, *35*, 74.

AM100043Q